Microgel structure-driven linear and non-linear mechanical properties of self-assembled microgel films

Eva Dieuzy[1,2,3], *Stéphane Auguste*[2,4], *Kamel Chougrani*[5], *Valérie Alard*[5], *Laurent Billon*[1,2,3] *
Christophe Derail[1,2] *

[1]*Universite de Pau et Pays de l'Adour, E2S UPPA, CNRS, Institut des Sciences Analytiques & de PhysicoChimie pour l'Environnement & les Matériaux, UMR5254, 64000, Pau, France*

[2]*LERAM, LabCom UPPA/URGO, Hélioparc, 2 avenue Angot, 64053 Pau, France*

[3]*Bio-inspired Materials group: Functionalities & Self-assembly, E2S UPPA, Hélioparc, 2 avenue Angot, 64053, Pau.*

[4] *URGO RECHERCHE INNOVATION ET DEVELOPPEMENT ; 42 Rue de Longvic, 21300 Chenôve, France*

[5]*LVMH Recherche Parfums et Cosmétiques ; 185 Av. De Verdun, 45804 St Jean de Braye, France.*

Abstract

Soft self-supported cohesive films were formed by self-assembly of pH- and thermo-responsive P(MEO_2MA-*co*-OEGMA-*co*-MAA) microgels without any preparation and/or post-treatments. Linear and non-linear mechanical properties of those films were characterized respectively by dynamic mechanical measurements at low strain and uniaxial extensional tests at high deformation. A relationship between the microstructure of microgels and the mechanical strength of microgel-based films was successfully established. Compared to microgels crosslinked with Oligo(ethylene glycol) diacrylate (OEGDA), microgels with N,N-methylenebisacrylamide (MBA) demonstrate a less crosslinked structure but especially a looser shell which enables the particles to better interpenetrate between one another and resist to higher deformation. Novel films were also designed by controlled mixing microgels and the synthesis side-product, namely water-soluble polymer, WSP, in a ratio with WSP content till 100%. Those films demonstrated promising mechanical properties due to the structural characteristics of the later. The later act as a lever to tune the elastic modulus of films without diminishing their resistance at strain thanks to its high molar mass and crosslinked structure revealed by Steric Exclusion Chromatography (SEC) measurements.

Keywords: microgels, particle-based films, dynamic mechanical measurements, linear, non-linear, structure-properties relationship

Introduction

Latexes consist of polymeric particles that are widely used in coating and adhesive applications thanks to their film forming abilities. Upon the simple evaporation of the solvent, the particles self-assemble to form a cohesive and transparent film. The cohesion of structured films is governed by the depth of chain interdiffusion and entanglements between adjacent particles known as coalescence.[1] One of the key requirement to allow chain mobility and promote diffusion is naturally to ensure a temperature well above the glass transition temperature during the film formation process. Yet, the rising interest in structured latex films goes beyond their film forming properties. In addition to the intrinsic properties of the polymer, the particulate structure provides many other parameters to tune according the targeted applications and mechanical properties. Indeed, each particle can be considered as a building block that is tunable in terms of size, structure and morphology. A gradient of crosslinking density within latex particles has demonstrated to greatly impact the mechanical strength of films.[2,3] In a like manner, blending soft with harder latexes has been extensively studied in view of increasing the film toughness.[4–6] Stimuli-responsive microgels, also called "smart nanoparticles" differentiate themselves from classical latex in their high swelling ability that responds to external stimuli such as temperature and pH.[7–10] Such microgels are widely investigated for their high potential in skincare, cosmetic and biomedical applications. Due to their high swelling and hydrophilic properties, the film formation of microgels is more challenging than latexes and often requires external binding to prevent the redispersion in contact with water. One of the most widespread techniques is known as the Layer-by-Layer assembly and consists of alternating oppositely-charged layers in order to create physical bonds between particles.[11–15] Another widespread technique for making dense microgel films is spin coating.[16–18] However, these techniques seem not suitable for skincare applications which require a material spreadable on skin that readily forms a "second skin" film *in situ*. On the other hand, very few studies have reported the self-assembly of microgels into cohesive films without any external (chemical or physical) action. Zhou *et al.*[19] reported the simple formation of (PNIPAM-NMA)-based microgel films by batch precipitation polymerization where the cohesion arose from the self-crosslinking of NMA units. More recently, Sonzogni *et al.*[20] designed (PVCL-PBA)-based microgel films on the simple solvent evaporation during which the PBA polymer promoted the chain interdiffusion needed to stabilize the films. The resulting thermoresponsive films exhibit interesting mechanical properties and low cytotoxicity. Along the same line, Boularas *et al.* reported the design of thermoresponsive and transparent P(MEO_2MA-*co*-OEGMA-*co*-MAA) microgel films.[21] The films were

qualitatively described as soft, cohesive and flexible: in sum, promising properties for skincare applications.

In a recent study from our group, it was demonstrated that tuning the crosslinker type and the crosslinking density can result in significant structural changes in the microgel microstructure.[22] Indeed, the structural analyses revealed that the N,N-methylenebisacrylamide (MBA) crosslinker generates an architecture with a less crosslinked shell and more dangling chains at periphery than with using poly(ethylene glycol) diacrylate (OEGDA) crosslinker.[23] Our group demonstrates that the microstructure in turn greatly influences the rheological properties of concentrated suspensions, especially the capacity of microgels to entangle and interpenetrate between one another. [24]

Taking a step further, the main objective of this paper is to quantify the mechanical strength of the P(MEO2MA-*co*-OEGMA-*co*-MAA) microgel-based films and understand to what extent the microgel microstructure impacts them. Moreover, we propose to pilot mechanical properties with the presence or the addition of a synthesis side-product, the water-soluble polymers.[22,2520] In this scope, the rheological and mechanical behaviors of P(MEO_2MA-*co*-OEGMA-*co*-MAA) purified microgel films were investigated in both the linear and non-linear domains and the structural deformation under elongation was observed at the microscopic scale using Atomic Force Microscopy. The second objective of the present study was to investigate the origin of the looser microstructure of MBA-crosslinked microgels while the crosslinker contents are set at 2 mol.% in both syntheses. One hypothesis was suggested: MBA crosslinker may react in a greater portion to lead to the synthesis side-products, namely water-soluble polymer chains that did not form finite particles, than with microgels compared to OEGDA crosslinker. The structural characteristics of the water-soluble polymers were analyzed for both MBA and OEGDA syntheses. Finally, the authors explored the properties of novel reformulated films by blending microgels and water-soluble polymers in controlled proportion.

Materials & Methods

Materials. Di(ethylene glycol) methyl ether methacrylate (MEO_2MA, 95%), oligo(ethylene glycol) methyl ether methacrylate (OEGMA, terminated by 8 EG units with Mn=475g.mol-1), methacrylic acid (MAA), poly(ethylene glycol) diacrylate (OEGDA, Mn=250 g.mol^{-1}), N,N-methylenebisacrylamide (MBA) and potassium persulfate (KPS) were purchased from Sigma Aldrich and used as received. Purified water from a Millipore Milli-Q system was used.

Microgel synthesis. The precipitation polymerization of microgels was carried out in a 2 L jacketed glass reactor by following the procedure previously described by Boularas *et al.*[26,27] Briefly, MEO_2MA (92.6 mmol), OEGMA (10.3 mmol) and varying amounts of crosslinker, either OEGDA or MBA, were dissolved in 930 g of water. The crosslinker ratios were set at 2 mol.% *versus* the total vinylic molecules, respectively corresponding to 2.12 mmol. The mixture was introduced in the 2 L reactor and stirring was set at 150 rpm. The reactor was purged with nitrogen for 45 min to remove oxygen at room temperature. MAA (5.41 mmol) was dissolved in 30 g of water and added to the reactor. The mixture was heated to 70°C. Finally, KPS (0.958 mmol) was dissolved in 40 g of water and inserted into the reactor to start the reaction. The reaction was kept at 70°C during 6 hours. At the end of synthesis, the colloidal suspension consists of microgel particles (70 wt%) and water-soluble polymer WSP (30 wt%) which did not fully react to form finite particles.

Film preparation.

Purified films. To study films formed from the assembly only of microgels, the suspensions are purified through 3 centrifugation cycles of 20 minutes at 20,000 rpm to extract the WSP. Then, films are formed by the straightforward water evaporation of purified solutions at 37±5°C in a bell jar oven. Silicone molds are chosen for an easy removal of the dried films.

Blended films. First, microgel particles and WSP are separated by centrifugation (20 minutes at 20,000 rpm). WSP is kept aside from the first centrifugation cycle whereas microgels receive 3 cycles. Solutions are concentrated by evaporation at about 3 wt.% for practical reasons. Solutions are mixed in controlled proportion and poured in silicone molds. Films are dried like classic microgel films. Five film compositions are compared for each crosslinker type (OEGDA and MBA) from 100 wt.% of microgels (classic purified films) to 100 wt.% of WSP.

Methods

Atomic Force Microscopy. Topographic images of the films are captured with a Bruker Multi mode 8 AFM. Peak Force QNM Air mode with ScanAsyst Air probes is chosen to scan films in dry environment. Probes have an average spring constant k of 0.4 $N.m^{-1}$.

Surface of films: Films are directly placed onto an AFM stainless-steel disk covered by a double-faced adhesive tape. ***Cross-section of films***: Neat cross-sections of thick films are performed with an ultra-cryo microtome apparatus Leica EM UC7, using a cryo-chamber Leica EM FC7 cooled down at -80°C. During surfacing, sample is maintained between two

Thermanox coverslips purchased from Thermo Fisher Scientific. ***Surface of stretched films:*** Films are manually subjected to uniaxial deformation and wrapped around a silicon wafer in their stretched state. Glue is applied on the bottom face of the wafer to maintain deformation but not in contact with the top face. The length between two dots is measured by ImageJ®, an image analysis software, before and after deformation to calculate the applied strain ε.

Rheological and mechanical analyses. Rheological analyses are performed on a MCR 302 rheometer from Anton Paar. The temperature is controlled with the oven chamber by forced dry air stream.

Linear shear measurements are performed on ≈ 1 mm-thick films with a 8 mm-parallel plates geometry. The linear regime is determined by performing a stress sweep from 0.001 to 100% at constant frequency equal to 1 Hz. The linear regime is established by the linearity between stress *vs* strain and can be assumed that G' has to be in a +/- 10% error margin. The frequency sweeps are carried out from 0.01 to 600 rad.s^{-1} with constant normal force of 0.2N and under a constant strain which is related to the temperature. Considering the structure of microgels as a continuum with WSP, one can apply the Time-Temperature Superposition (TTS) equivalence. Frequency sweeps are performed from -10°C to 50°C with thermal step of 10°C. To ensure the linear regime, strain is set at 1% for temperatures from 50°C to 10°C, at 0.1% for 0°C and at 0,01% for -10°C. Master curves were obtained by shifting horizontally the frequency sweeps performed at various temperatures in order to fit the frequency sweep performed at 20°C. The vertical translation is neglected for this low temperature range. Here, the empirical relationship of Williams-Landel-Ferry (WLF) expressed by Eq. (1) does not apply as films are made from crosslinked copolymers.[28]

$$\log(a_T) = -\frac{C_1(T-T_{ref})}{C_2+(T-T_{ref})} \qquad (1)$$

with C_1 and C_2 empirical constants and T_{ref} the reference temperature. For information only, curves from the logarithmic values of shifting factors as a function of temperature are fitted with the WLF equation. The best fit is obtained for C_1= 8.86; and C_2=101.6 taking T_{ref}= 20°C.

Extensional rheology at large deformation is performed by using a SER (Sentmanat Extension Rheometer) geometry which consists of paired windup drums that move in equal but opposite rotation. The geometry doesn't require to clamp the specimen between grips and is particularly appropriate for soft and thin polymer films. Test temperature is varied from 20°C to 50°C with no control on the relative humidity. Film dimensions are in the following range: 0.5-1 mm x 1-2 mm x 15-20 mm. Films are extended until rupture with a constant

strain rate, also referred to as the Hencky strain rate $\dot{\varepsilon}_H$. The extensional viscosity curves always represent the average from at least five specimens tested in the same condition. Error bars in the Y-axis indicate the standard deviation on the extensional viscosity. The point of rupture corresponds to the average in extensional viscosity but also in time from all the specimens tested. The logarithmic strain, or Hencky strain ε_H, is function of $\dot{\varepsilon}$ the constant strain rate, t the time, L the sample length at instant t and L_0 the initial sample length as given by equation (2).

$$\varepsilon_H = \dot{\varepsilon} \times t = \ln (L/L_0) \qquad (2)$$

Tensile tests are performed on a texture analyzer TA.XT Plus from Stable Micro Systems at a speed of 1 $mm.s^{-1}$. Film dimensions are in the following range: 150-200 µm x 10 mm x 30 mm. Young's modulus is calculated from the elastic region derived from the first linear slope of the stress-strain curve which here corresponds to strain from 0 and 8%.

Steric Exclusion chromatography (SEC) apparatus consists of a set of aqueous columns from Shodex and an Agilent 1260 Iso pump from Agilent technologies. The set-up is further described elsewhere.[29] The apparatus is coupled with a Multi Angle Light Scattering (MALS) and a differential refractometer detector (RI). The MALS detector is a Dawn Heleos detector from WYATT Technology. The RI detector is an Optilab T-rEX from WYATT Technology operating at a laser wavelength of 664 nm. During the experiment, the flow rate is set on 0.5 mL/min and the column temperature is fixed at 30°C. The mobile phase consists of an aqueous solution of $NaNO_3$ at 0.1 $g.mol^{-1}$ (8.2 $g.L^{-1}$), and azide sodium NaN_3 (0.1 $g.L^{-1}$) as eluent, stabilized with a buffer at pH 8. Before use, the mobile phase is filtered at 0.1 µm. The solutions of water-soluble polymers are prepared at a concentration of 500 ppm in a buffer of pH 8, from which a volume of 100 µL is injected. Before use, the solutions are filtered at 250 nm to remove any impurities and eventual microgels. Data were analyzed by using a Zimm model on Astra 6.1 software. The detection limit of the equipment for the radius of gyration is ≈ 10 nm.

Results and Discussion

OligoEthyleneGlycol microgels were synthesized as previously described by our group.[22,26] Indeed, such OEG-based microgels were described to present the interesting property to be self-assembled *via* simple solvent evaporation process at surface skin temperature and ambient pressure. They spontaneously form a self-assembled and self-supported transparent

film without any external triggers or post-reactions.[21] Herein, two different approaches were developed based on purified microgels and reformulated microgels with various wt% of WSP.

Microstructure of purified microgels films

Height mappings were performed by AFM on the top surface as well as on cross section of microgel films in order to study the self-assembly of microgels. Figure 1 (a) shows a mapping of top surface of 2-MBA crosslinked films whereas Figure 1 (b) and (c) show the mapping of the cross-section of 2-MBA films. Corresponding AFM mappings of OEGDA-crosslinked films are found in Figure S1.

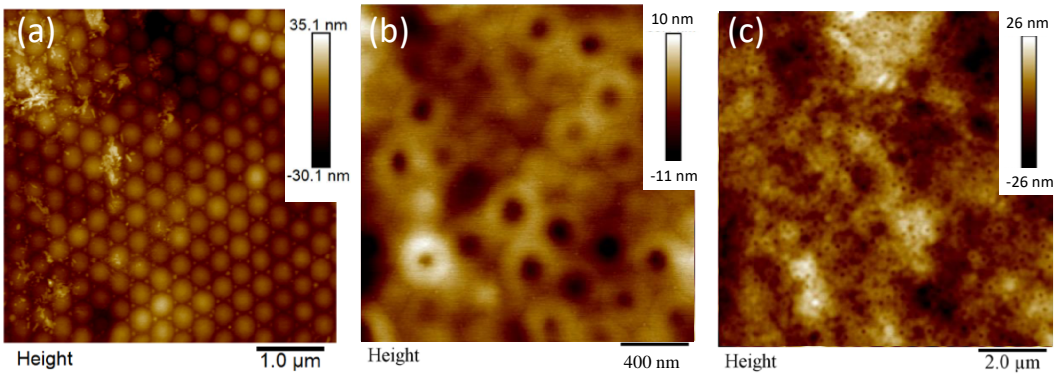

Figure 1. AFM height mappings of microgel films crosslinked with 2 mol.% MBA (a) 5µm x 5µm scan of top surface (b) 2µm x 2µm scan of cross section (c) 10µm x 10µm scan of cross-section. Corresponding AFM mappings for OEGDA-crosslinked films are shown in SI.

It is observed from Figure 1 (a) that the top layer of microgel particles self-assembles into a perfect hexagonal-close-packed *hcp* array. One can observe from the three images that the particles do not significantly coalesce and keep their spherical shape. Yet, the images reveal a continuous phase around the lighter part that is comparable to a matrix. One can assume that the soft and loosely crosslinked shells of microgels have inter-diffused between one another to form this continuous phase whereas the lighter, *i.e.* higher parts corresponds to the more crosslinked part of microgels, *i.e.* the core. One can observe from Figure 1 (b) and (c), which correspond to the bulk of the film, a more disordered assembly through the thickness of the film but with some evidence for a hcp array in the entire thickness of the films. A height difference of ≈ 15 nm between core and shell is also observed showing a "donuts" shape. This "donuts" shape could arise from the presence of water molecules non-homogenously distributed within the microgels due to the core-shell structure. As one knows, microgel films

contain and absorb water from their environment due to their hydrophilic properties and low glass transition temperature OEG-based microgels, especially. Indeed, Aguirre *et al.* described after drying of the films, the presence of some water molecules (~15 wt% by TGA measurements) due to the spontaneaous wet adsorption from air.[25] In particular, the passage from the cryo microtomy sectioning at -80°C back to room temperature certainly makes them gain a significant amount of water. Thus, microgels could be swollen in an uneven way due to their non-homogeneous crosslinking distribution. Another hypothesis could be that the dense cores were snatched from the films during cross-sectioning due to their higher rigidity, leading to this "donuts" shape.

Rheological and mechanical behavior of purified microgel films

As established by the pioneering work of Zosel and Ley and supported by many subsequent studies, latex-based films with a particulate crosslinked structure commonly exhibit a viscoelastic response similar to continuously crosslinked films due to the presence of partial chain inter-diffusion across particle boundaries.[30–33] As a consequence, some basic concepts from homogenous networks can be applied such as the time-temperature superposition (TTS) principle which allows to access broader frequency ranges.[28,34] Hence, dynamic mechanical behavior in the linear regime of purified microgel films was explored through frequency sweeps at several temperatures. Master curves built at 20°C for purified microgel film crosslinked with 2 mol. % of MBA and 2 mol.% of OEGDA are respectively shown in Figure 2 A and B. The logarithmic values of the TTS shifting factors a_T *versus* temperature are inserted in Figure 2 (A) and (B).

By reaching higher frequencies, the master curve allows to observe the transition from the rubber plateau to the glassy region. The glass transition is indicated by two crossover points of *G'* and *G''* which are located respectively at about 10 rad.s^{-1} and 3x10^3 rad.s^{-1} for both crosslinkers. This finding points out that the glass transition occurs at the same frequency, or equivalently at the same temperature, regardless of crosslinker type. It was expected as the crosslinker remains in very small proportion (2 mol.%) compared to polymer content.

The master curve also refines the value of *G'* at the rubber plateau by reaching lower frequencies. The typical G'-G'' cross-over indicating the transition from the rubber plateau to the flow region for thermoplastic polymers is not observed in this range. The absence of flow may reveal that there are no disentanglements of polymer chains at the scale of the particle

neither disentanglements between microgels. While no disentanglement within microgel particle is expected due to crosslink points, the absence of slippage between microgels can be explained by some strong physical entanglements of chains between neighboring particles. As reported by many studies on particle-based latex films, dynamic mechanical measurements at low strain do not differentiate particulate networks from homogenous networks when exists the presence of partial chain inter-diffusion across the particle boundaries. [30,31] Nonetheless, one can suggest the flow region might have been visible by accessing even lower frequency. Yet, lower frequency means higher temperature which would have led to the change in microstructure as well a considerable loss of water from these temperature-dependent and highly hygroscopic microgels presenting a VPTT transition.[22,26,27] From the reading of the master curves, the storage moduli at the rubber plateau (10^{-3} rad.s^{-1}) are about 6.10^4 Pa and 9.10^4 Pa for OEGDA and MBA films, respectively. Since these microgel films are hygroscopic and the relative humidity rates during the tests cannot be controlled, the standard deviation has been assessed on films with different storage times and films casted from different microgel syntheses (Table 1).

Although OEGDA films seem to exhibit higher values of *G'* and *G''* than MBA ones, yet the difference seems to be non-significant considering the relative large standard deviation. In conclusion, one can note that the two systems exhibit very similar dynamic rheological responses and the crosslinker type does not induce significant differences in the linear regime. Both microgel-based films behave as a continuously crosslinked film in spite of their particulate structure of self-assembled soft colloid spheres.

Table 1. Storage and loss moduli for purified P(MEO_2MA-*co*-OEGMA-*co*-MAA) microgel films crosslinked with 2 mol.% MBA and 2 mol.% OEGDA.

	2 mol.% OEGDA	**2 mol.% MBA**
***G'* (*10^4 Pa)**	8 ± 4	4 ± 2
***G''* (*10^4 Pa)**	1.1 ± 0.5	0.6 ± 0.2

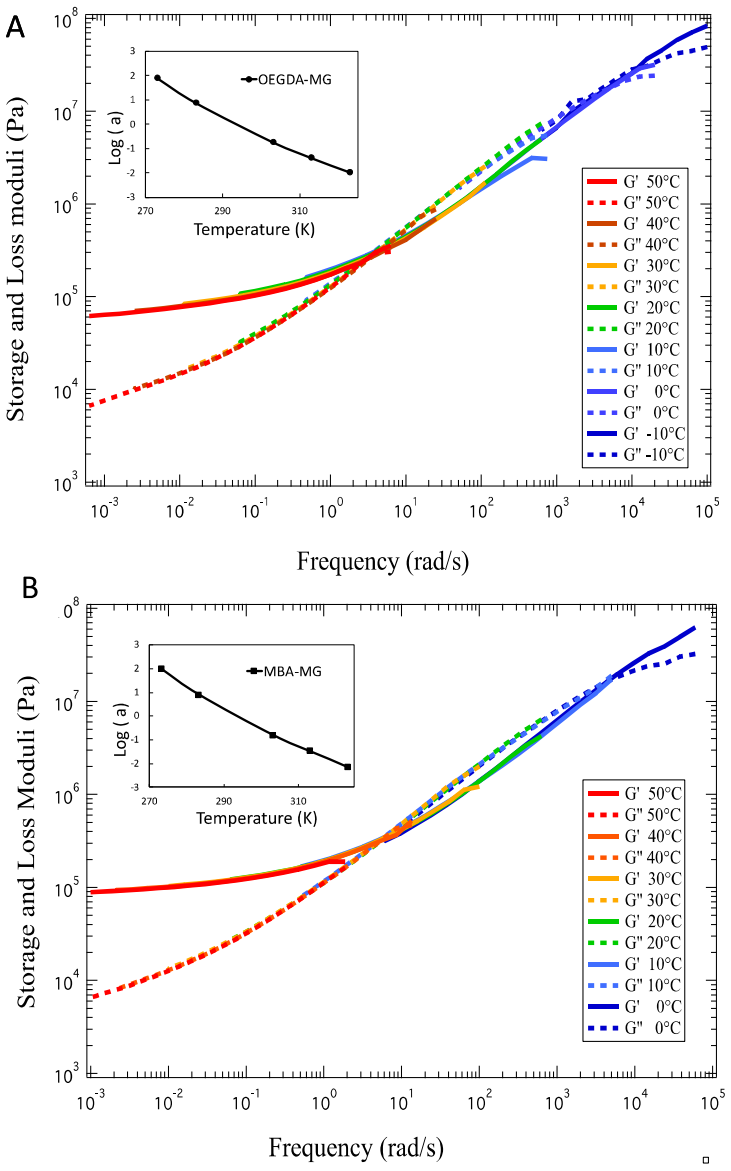

Figure 2. Master curves at T_{ref}=20°C. Storage modulus G' (solid line) and loss modulus G'' (dashed line) *versus* frequency for purified microgel films crosslinked with (A) 2 mol.% OEGDA (B) 2 mol.% MBA. The temperature-dependency of the logarithmic shifting factors are inserted in the graph of the corresponding sample.

Dynamic mechanical measurements were complemented with uniaxial tests as the later can generate a much higher degree of molecular orientation than simple shear in the linear domain. Thus, it can bring additional information regarding the chain disentanglement and may differentiate the two types of films. Extensional rheology represents one type of uniaxial elongation tests during which the specimen is pulled at a constant Hencky strain rate $\dot{\varepsilon}$ contrary to traditional tensile tests where the crosshead speed is set constant.[35] The average

extensional viscosity *versus* time for OEGDA and MBA-crosslinked microgel films are reported in Figure 3 (a) for a Hencky strain rate of 0.5 s^{-1} at 20°C. Figure 3 (b) and (c) respectively show a film at rest before test and in its stretched state just before the rupture on the SER geometry.

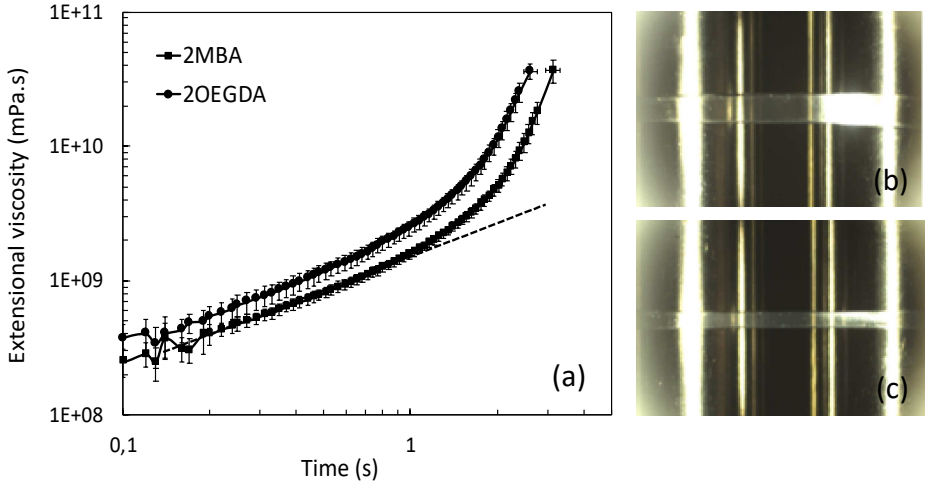

Figure 3. Average extensional viscosity *versus* time of purified P(MEO_2MA-*co*-OEGMA-*co*-MAA) microgel films crosslinked with 2 mol.% OEGDA and 2 mol.% MBA at 20°C. Strain rate was set at 0.5 s^{-1}. Dashed line represents the linear viscoelastic response described by $\eta_E = 3x\,\eta*$. Film before the test (b) and just before the rupture (c).

For both systems, the extensional viscosity steadily increases at first following the linear viscoelastic response that relates the extensional viscosity η_E to the complex shear viscosity η^* as given by Eq. (3). The multiplicative constant, referred to as the Trouton ratio *Tr* is set at 3 for extensional flow. The linear response from Eq. (3) is represented by the dashed line in Figure 3.

$$\eta_E = Tr\ x\ \eta* = 3x\,\eta* \qquad (3)$$

MBA films exhibit lower values of extensional viscosity than OEGDA ones. It may be explained by lower values of *G'* and *G''* measured in the linear regime for MBA films (Table S1). At Hencky strains greater than 0.5, or equivalently time superior to 1 s, the experimental extensional viscosity deviates and increases faster than the linear response. This upward deviation is referred to the so-called strain-hardening and commonly occurs in chemically crosslinked as well as branched polymers. It is characteristic of the chain-branching architecture as well described in the literature.[36–40] The chain entanglements start to resist to

extension whenever the limit of chain extensibility is approached and cause the stiffening of the network. As a result, the extensional viscosity follows a rapid upward increment with elongational time. Herein, strain-hardening is suspected to be caused by both the crosslinked points within microgels and the strong physical entanglements between neighboring microgel particles. The strain at rupture was calculated by multiplying the time at rupture by the strain rate used, Eq. (2). Contrary to the small amplitude oscillatory shear measurements, a significant difference emerges from the two crosslinkers used in the non-linear deformation domain. Indeed, MBA films break at 157 ± 9 % whereas OEGDA ones break at 131 ± 7%. Aside, the use of different Hencky strain rates (1, 0.5 and 0.1 s^{-1}) seems to not influence on the strain at rupture as observed in Table S1.

The network of MBA-crosslinked microgels demonstrates a higher resistance to stress compared to OEGDA ones. This finding echoes the results recently reported by our group on these systems in their suspension form.[23] Indeed, the structural analyses revealed that MBA crosslinker generates an architecture that is more suitable for interpenetration between particles namely a less crosslinked shell and more dangling chains. As a consequence, concentrated suspensions of MBA microgels developed a much higher yield stress than OEGDA ones due to better chain entanglements between close packed particles. In like manner, once films are formed, MBA-crosslinked microgels are better entangled between one another at their interfaces which results in higher strains at rupture.

In addition, the impact of the temperature of formation was assessed for films formed at 20°C, 32°C, 37°C and 60°C (Figure 4). Indeed, microgels immersed in aqueous solvent can either be swollen or collapsed due to their thermoresponsive property, *i.e.* the VPTT. The objective was to evaluate whether the state of microgels impacts the quality of the assembly during the film formation, *i.e.* whether swollen microgels inter-diffuse more between neighboring particles than collapsed particles.

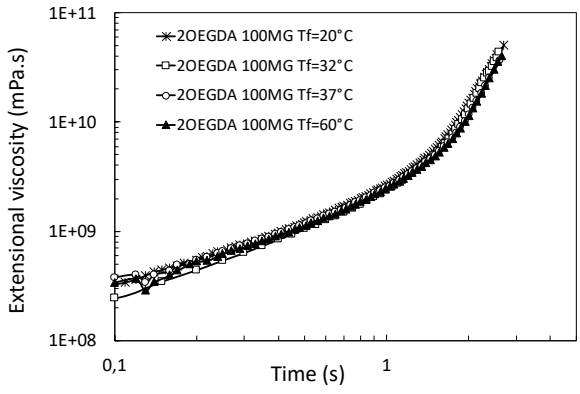

Figure 4. Extensional viscosity *versus* time of 2-OEGDA microgel film tested at 20°C with Hencky strain of 0.5 s^{-1}. Films were formed at different temperatures: 20°C, 32°C, 37°C and 60°C.

The temperature of formation has clearly no impact on the extensional viscosity neither the strain at rupture. Whether the microgel films are formed under (20°C), within (32°C, 37°C) or above the VPTT (60°C), the Hencky strain at rupture remains equal to 133 ± 2 %. The polymer chains may keep some mobility at 60°C which enable the microgels to interpenetrate between each other in their collapsed state. Indeed, it was previously described in other studies that microgels still contain a non-negligible content of water when they are in their collapse state.[9,41,42] The water is essentially located in the shell providing mobility to the external dangling chains which are the main responsible for the inter-diffusion. In addition, microgel films are stored and tested at room temperature, without control of hygrometry, once formed. Chains may have time to relax and inter-diffuse at microgel boundary thanks to their solid-like viscoelastic behavior.

Uniaxial tensile tests were performed and compared to the extensional viscosity measurements. The stress *versus* strain curves for OEGDA and MBA-crosslinked microgel films are reported in Figure 5. Young's modulus, the tensile strength (equivalent to the tensile stress at break in this case), the strain at break and the fracture energy were extrapolated from the curves (Table S2).

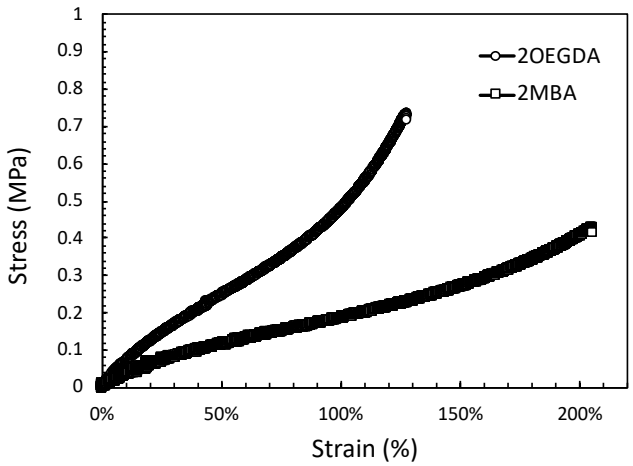

Figure 5. Stress-strain curves of OEGDA and MBA-crosslinked microgel films performed at a crosshead speed of 1mm.s^{-1} at 20°C.

The tensile behavior of both films is characteristic of elastomers, *i.e.* polymers that exhibit a rubber-like elasticity and require a high force to break, principally due to strain-hardening.[43] Similarly to extensional viscosity, strain hardening arises from the resistance to polymer chain alignment. It is clearly observed that MBA films are definitely softer than OEGDA films which results in a lower Young's modulus and lower tensile strength. It corroborates with the lower extensional viscosity values and the lower shear modulus measured in the linear regime. In agreement with the extensional viscosity, MBA films exhibit a much higher elongation at break than OEGDA ones at 201 ± 24% and 127 ± 15%, respectively. The fracture energy *i.e.* the toughness of MBA films is identical to OEGDA films (0.39 MJ.m^{-3}) which arises from the opposite effects of a lower tensile stress but a higher strain at break. The Hencky elongations at break from the extensional viscosity measurements were converted to engineering strain with Eq. (5) to be compared with the tensile elongations at break.

$$e = \exp(\varepsilon_H) - 1 \qquad (5)$$

where e is the engineering strain defined by the change in length ΔL per unit of the initial length L_0.

The converted engineering strains at break from extensional viscosity are 270% and 395% for OEGDA and MBA films, respectively. These values are much higher than the tensile strains. The discrepancy can be attributed to the tensile geometry that is less suitable for soft and thin polymers. The jaws firmly squeeze the thin films which often leads to a premature fracture

located below the grips and not ideally at the middle of the specimen. This observation confirms that the elongational properties of soft and viscoelastic films were preferentially evaluated by extensional viscosity thereafter.

Young's moduli and tensile strengths of these films are relatively low compared to the ones reported in the literature for other free-standing microgel films elaborated without post-crosslinking techniques.[20,44] For instance, Sonzogni *et al.* obtained Young's modulus and tensile strength of 84.2 MPa and 10 MPa respectively for P(VCL-BA) thermoresponsive microgel films.[20] Nonetheless, low Young's modulus and tensile strength are desired properties in regard of the potential applications targeted *i.e.* skincare products. Indeed, materials designed for skincare have the paramount requirement to exhibit very similar mechanical properties to the skin ones in terms of elasticity, flexibility and elongation to form an ideal "second skin".[45–47] Although the mechanical properties of human skin are subject to a large variability, the values found in the literature for the Young's modulus ranges from 0.01 - 2 MPa.[48] Consequently, Young's moduli measured for these films, between 0.35 MPa and 0.65 MPa, are perfectly appropriate for skincare applications. In addition, their elongation at break is much superior to the skin one generally measured below 60%.[49,50] Hence, P(MEO_2MA-*co*-OEGMA-*co*-MAA) microgel films seems to exhibits very suitable mechanical properties for potential skincare applications.

To better understand the arrangement of microgels during deformation, films were observed by AFM in a static stretched state. Figure 6 shows the mappings of MBA films (a) at rest (b) under 30% of strain and (c) under 70% of strain. Similar AFM mappings for stretched OEGDA films are shown in Figure S2.

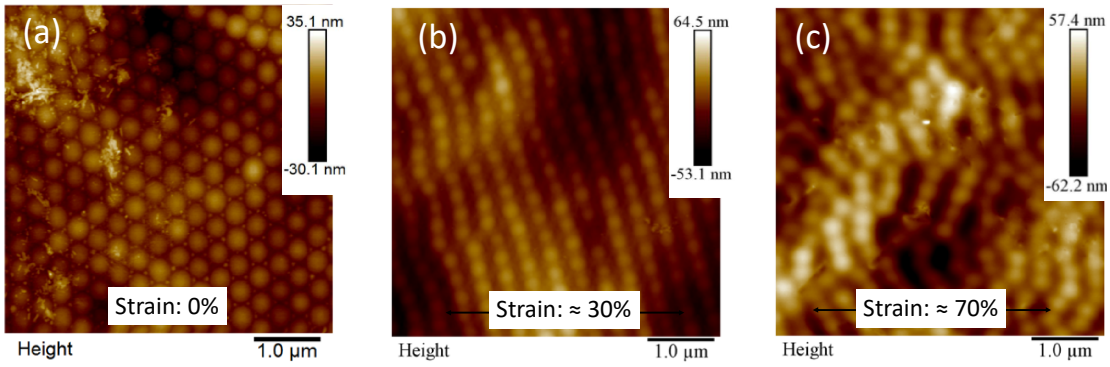

Figure 6. AFM micrographs performed on MBA-crosslinked films subject to different strains (ε): (a) ε=0%, 5 µm scan (b) ε=30%, 5 µm scan (c) ε=70% 10 µm. The stretching direction is parallel to the X axis of the AFM micrograph.

The stretching causes the loss of the hexagonal compact packing of the particle network. Under small deformation ($\varepsilon \approx 30\%$), we observed the alignment of the microgels, more specifically of their cores, in the perpendicular direction of elongation. The distance between two particles is larger than at rest but the cores are not significantly deformed and maintain a spherical shape. It suggests that, at this strain, the deformation mechanism is mostly located at the microgel interface where the entangled chains from the shell stretch to accommodate the stress. Lepizzera *et al.*[51] previously observed a similar deformation pattern on core-shell latexes where the dense core was made from PMMA and the soft shell from P(MMA-*co*-BA-*co*-AA). The authors explained the formation of these "necklaces" from the shrinking of the film width during elongation that pushed the particles closer in the Y direction and further in the X direction. The deformation only occurred in the matrix made from a softer copolymer than the core. Under further elongation ($\varepsilon \approx 70\%$), the structured alignment disappears and is replaced by zig-zags or chevrons (Figure 6c). In addition, cracks are visible by deep gap in the Z direction. The simple deformation of the soft shell is not sufficient anymore to accommodate the stress at large elongation and other deformation mechanisms are at stake. These chevrons and cracks were also observed in the AFM mappings of Lepizzera *et al.*[51,52]. One can conclude that our systems behave very similarly to composite structured latex films, where the loosely-crosslinked shells represent the soft matrix and the dense cores are comparable to hard fillers.

The influence of the test temperature on the film elongational properties has also been evaluated to bring additional knowledge on the chain dynamics at the microgel interface. Figure 7 (a) and (b) respectively show the average extensional viscosity curves of 2-MBA and 2-OEGDA films for test temperatures of 20°C, 32°C and 50°C.

As an evidence from the relationship between the complex viscosity and the moduli (Eq. (3) and (4)), for both MBA and OEGDA films, one observes that the extensional viscosity is lower at higher temperature.. 2-MBA films exhibit a similar elongation at break at 20°C, 32°C and 50°C corresponding to ≈ 160 %. The deformation mechanism in the non-linear regime, mostly governed by the stretching of the dangling chains at the microgel interface as observed by AFM, remains identical regardless of the temperature change. Such conclusion cannot be drawn for 2-OEGDA films as observed in Figure 7b. The fracture type evolves from brittle to ductile with the presence of necking at higher temperature (insert in Figure 7b). With the hypothesis of shells from OEGDA microgels being less entangled with one another, one can suggest that the temperature better favors the disentanglements of the chains by slippage at

the microgel interface leading to a ductile fracture. In the case of MBA particles, one can suppose that the temperature provided is not sufficient to disentangle the long chains that may have greatly inter-diffused between microgels. Thus, at their maximum elongation, the majority of chains breaks instead of slipping which may result in a brittle fracture.

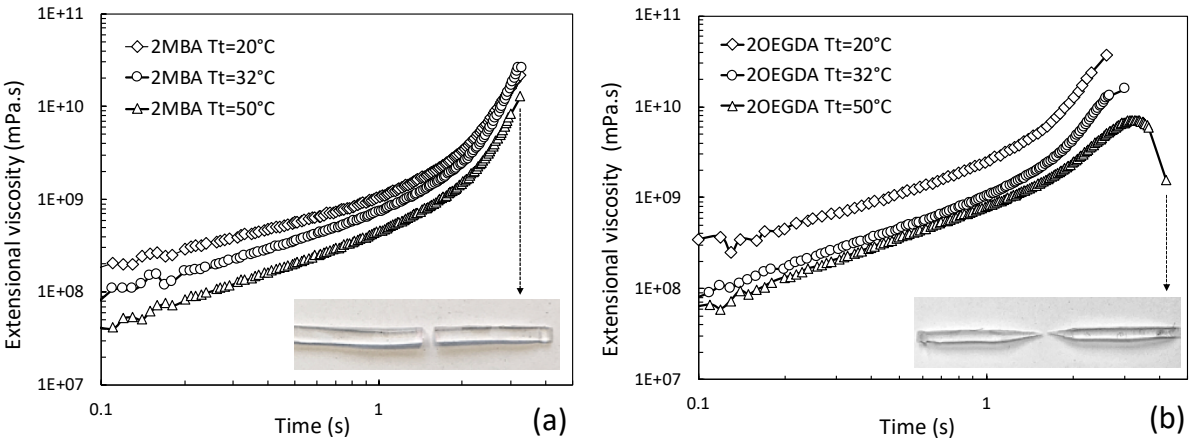

Figure 7. Extensional viscosity *versus* time of P(MEO2MA-co-OEGMA-co-MAA) microgels crosslinked with (a) 2 mol.% MBA and (b) 2 mol.% OEGDA for different test temperatures: 20°C, 32°C and 50°C. Inserted pictures show the films after rupture for T_{test}=50°C.

The previous study on purified microgel suspensions as well as the present results on purified films have revealed that microgels crosslinked with 2 mol.% MBA have a lower crosslinking density than OEGDA-crosslinked ones. The looser structure enables a better inter-diffusion of microgels between one another leading to higher yield stress for suspensions and higher strain at rupture for films. In addition, MBA films are softer than OEGDA ones, revealed by the lower elastic modulus. The crosslinking content being set at 2 mol.% in both cases, the author wished to investigate whether a greater portion of crosslinker was reacting with the synthesis side-products *i.e.* water-soluble chains, in the case MBA crosslinking. Structural analyses were then performed on both water-soluble polymers.

Structural characterization of the Water-Soluble Polymer (WSP)

Size Exclusion Chromatography (SEC) measurements coupled with a Multi-Angle Laser Light Scattering (MALLS) detector were performed on OEGDA and MBA-WSP to assess their absolute molecular weight. Measurements were also performed on a linear PEG (M_w = 35,000 g.mol^{-1}) in order to have a reference of a well-defined linear polymer. Figures S3 (a) and (b) respectively show the molar mass and root-mean-square *rms* radius (or equivalently the gyration radius R_g) as a function of the elution volume.

PEG 35K has a weight average molar mass M_w at 34,000 g.mol^{-1} which validates the reliability of the method used. As expected, the commercial PEG polymer has a very narrow distribution with a dispersity value $Đ$ of 1.01. OEGDA and MBA-WSPs have in common a similar population of molecular masses ranging from 1x10^4 to 1x10^5 g.mol^{-1}. Yet MBA-WSP has a significant proportion of much higher molecular masses ranging from 1x10^5 to 1x10^6 g.mol^{-1}. As a result, MBA-WSP has a molar mass of 103,000 g.mol^{-1} compared to 51,000 g.mol^{-1} for OEGDA-WSP (Table 2). Conversely to what is reported in some other studies,[53] both water-soluble polymers do not correspond to the size of oligomers but to a high molecular mass polymer.

Table 2. Molecular masses in number (M_n), in weight (M_w) and dispersity index ($Đ_M$) for PEG (35,000 g.mol^{-1}), OEGDA-WSP and MBA-WSP for a synthesis with 2 mol.% of crosslinker

	PEG35K	**OEGDA**	**MBA**
M_w (kg.mol^{-1})	34	51	103
M_n (kg.mol^{-1})	33	34	37
$Đ$	1.01	1.6	2.8

Both WSP exhibit a radius of gyration ≈15 nm in average which demonstrates the water-soluble polymer must have a highly branched and/or crosslinked structure considering their high molecular masses. The higher molar masses from MBA-WSP reach gyration radii up to 30 nm, indicating bigger but not necessarily denser objects. These results support the idea that a portion of the crosslinker does not react with the growing microgel particles but creates water-soluble polymer in solution. In addition, the presence of higher molecular masses for MBA-WSP reinforces the hypothesis that a higher amount of MBA crosslinker reacts with the free soluble chains leading to lower crosslinked MBA microgels than OEGDA ones. The conformational plot, *i.e.* the gyration radius *versus* the molecular weight, is then represented for OEGDA-WSP, MBA-WSP and PEG 35K (Figure 8). Indeed, the dependence of the molecular mass with a physical quantity such as the intrinsic viscosity or the radius of gyration reveals important information on the internal structure, the stiffness and the branching of macromolecules. The relationship can be described by a power law in a specified range of molecular weights such as:

$$R_g \propto M_w^{\alpha} \qquad (6)$$

It may be beneficial to recall the theoretical expectation of exponent α for the shape of basic entities: 0.5 for the random coil conformation of flexible linear polymers in Θ-solvent and 0.33 for spherical particles of uniform density.[54] A representative power law $R_g \propto M_w^{0,6}$ was added in Figure 8 to represent a theoretical linear polymer in good solvent.

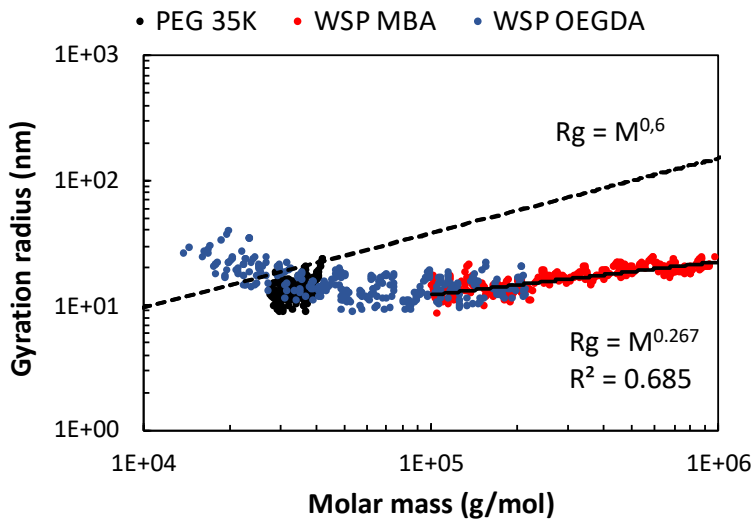

Figure 8. Conformational plot for (red) MBA-WSP, (blue) OEGDA-WSP, (black) PEG35K. Dashed line represent the dependence of a theoretical linear polymer with the power law: $R_g \propto M_w^{0,6}$

As previously mentioned, the linear PEG 35K (black dots) has such a narrow distribution in mass that it is not possible to fit the radius of gyration by a power law. Only MBA-WSP was fitted by a power law since it is the population with the clearest and broadest variation. The value of power law exponent from the fit was found to be $\alpha \approx 0.27$ with a coefficient of determination R^2 equals to 0.685. While the fairly low value of R^2 underlines the scatter around the regression line, one should interpret the α value with caution. Nevertheless, one can comment that the power law exponent is indeed closer to the theoretical value of spherical particles ($\alpha = 0.33$) than to the one of the random coil conformation of linear polymers ($\alpha = 0.5$). Thus, the water-soluble polymers formed during synthesis seem to present a rather nanogel-like structure which supports the initial hypothesis of highly branched and/or crosslinked polymers with high molecular masses. In further works, SANS measurements could be envisioned to quantify the degree of branching compared to the crosslinking density.

Rheological and mechanical behavior of formulated microgel films

In the light of the interesting structure of the water-soluble polymer, the mechanical properties of films composed of both microgels and the later were investigated. Five films were formed following different blend compositions: 100 wt.% of microgels (classic purified film), 100 wt.% of WSP and 75/25, 50/50, 25/75 wt.% of microgels/WSP ratio.

The inner structure of blended films was first observed with AFM performed on the surface of the film cross-sections. Figures 9 (a), (b) and (c) show mappings with the height channel of films composed of 25, 50 and 75 wt.% of microgels (MG), respectively. Figures 9 (d), (e) and (f) show mappings with the logDMT modulus channel of the corresponding films, which displays the stiffer regions in lighter colors and the softer in dark ones.

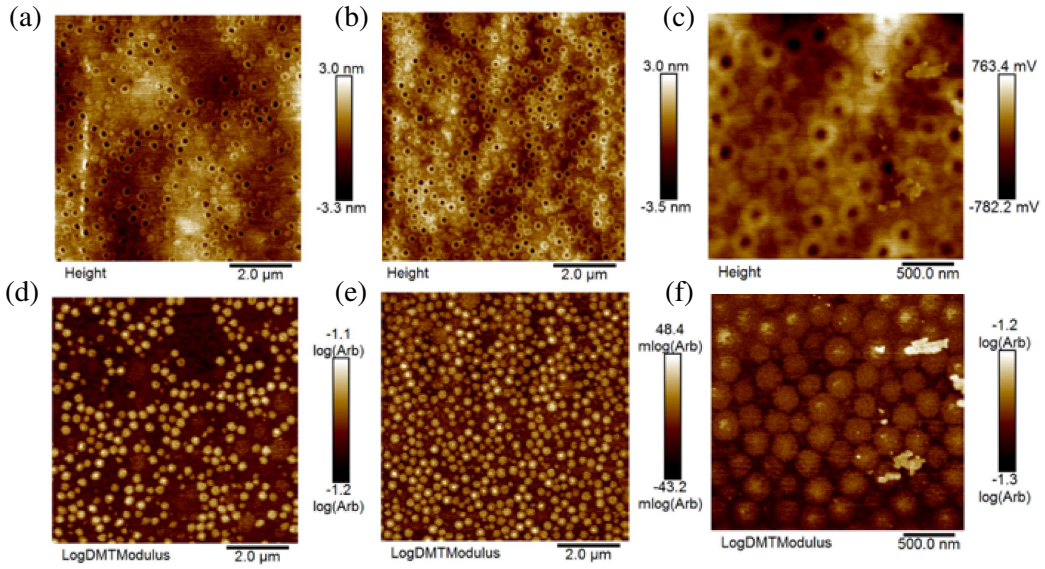

Figure 9. AFM **(left)** height and **(right)** LogDMT Modulus mappings of 2 mol% MBA-MG films for 75% MG

As one expected, the modulus mappings indicate that microgels are denser than the water-soluble polymer and resemble to hard spherical fillers dispersed in a soft composite matrix. Microgels are quite homogeneously distributed and dispersed without any aggregates, yet no structured arrangement is observed. Here again, the “donuts” structure is well observed with a clear gradient in modulus and height between the cores and the shells. The looser and probably more swollen shells are characterized by a greater height and a lower modulus than the dense cores. Furthermore, a gradual transition is observed between the microgel shells and the WSP matrix which suggests a similar structure as well as a certain interpenetration

between the two phases. Yet, the WSP matrix exhibits a lower modulus than the microgel shells (Figures 9 (d), (e) and (f)).

The rheological behavior of blended films was investigated with small amplitude oscillatory shear measurements and extensional viscosity tests at large deformation. Figure 10 shows the storage and loss moduli *versus* frequency and the average extensional viscosity *versus* time for MBA blended films. Corresponding curves for OEGDA blended films are reported in Figure S4. The Hencky strain and the extensional viscosity, both at break, were extrapolated from the extensional curves and plotted in Figures S5.

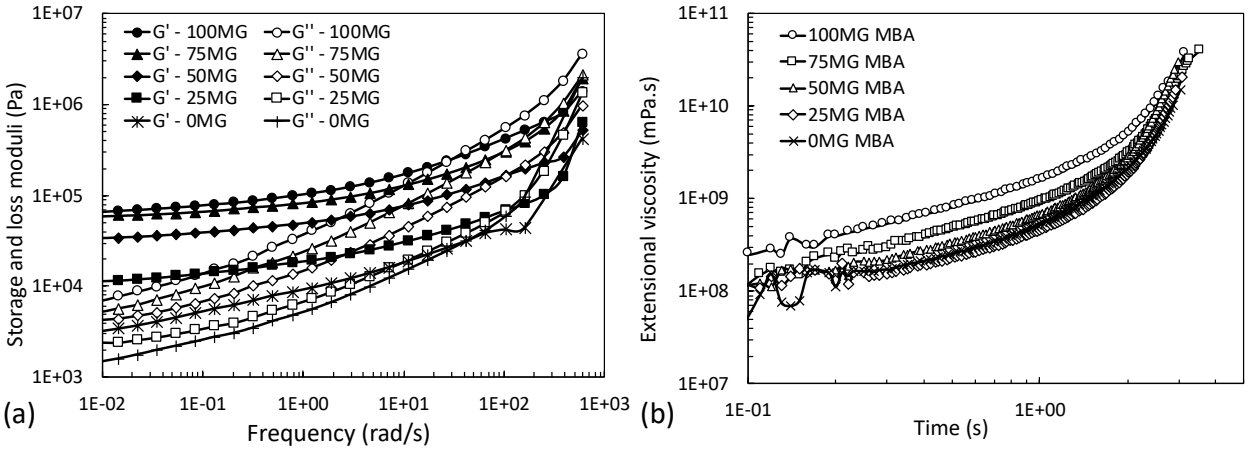

Figure 10. (a) Storage and loss moduli *versus* frequency at 20°C (b) Average extensional viscosity *versus* time for MBA blended films at 20°C for a Hencky strain rate of 0.5 s^{-1} with microgel and WSP contents inversely varying from 0% to 100%.

As the microgel content decreases, one can observe the drop of both G' and G'' moduli which indicates the films become softer and more viscous. For example, the storage modulus at 0.01 rad.s^{-1} of MBA films drops from 66 kPa to 3.2 kPa for 100% microgels to 100% of WSP. The drop-in moduli arises from microgel particles being driven further away from another due the incorporation of the WSP phase. In addition, a loss of crosslinking points occurs with the rising proportion of WSPs. As a consequence, the elastic plateau of 100% MBA-WSP films is not reached because of being shifted to lower frequencies. This can be quantified by the increase of the power law exponent from the relationship $G' \propto \omega^{\alpha}$ where $\alpha = 0.18$ for 100% WSP compare to $\alpha = 0.06$ (near 0) for 100% MG.

As a direct consequence of the decrease in G' and G'' with lower microgel content, the extensional viscosity also drops with decreasing MG%. . Nonetheless, all the films demonstrate strain-hardening and break at similar strains which is surprising for films composed of a prevalent proportion of WSPs (*e.g.* 75 and 100%) (Figure S5a). Indeed, it is

rather uncommon to obtain such high elongation properties for a film made only from a synthesis side-product since polymers rarely reach such high molecular masses and branched structures. All MBA blended films demonstrate a strain at rupture close to 155 % in average except the blend with 75% microgels which exhibits a higher value (≈ 180%) but the difference may not be significant considering the standard deviation. The preservation of the elongational properties for the lower WSP content may be attributed to the presence of strain hardening which is in turn a result of the branched and/or crosslinked structure of WSP. In addition, we recall that the very similar chemical nature of microgels and WSP must provide an excellent compatibility of the two components and strengthen their interface. MBA blended films break at much higher strain than OEGDA ones, regardless of the microgel-WSP composition. This was expected for blends with a prevalent proportion of microgels from the results of the first section. The same observation is made for films formed from 100% of WSP and the explanation lies in the structural characteristics of the latter. The analyses from size exclusion chromatography have highlighted a higher molecular mass for MBA-WSP. The higher molecular mass leads to higher strains at break.

Regarding the usefulness of self-assembled microgel films, *i.e.* raw or purified ones, they also present the ability to encapsulate/release high amounts of hydrophilic/hydrophobic active molecules.[25] Moreover, the viscoelastic properties of blended films lead to auto-adhesive properties which can be piloted by the formulation.[46,47] From the point of view of the future use of these self-assembled microgel films, considering these properties, they would be used as delivery patches systems or protective films for skin applications. Indeed, similar films behaves as super encapsulation/release devices of active cosmetic molecules, i.e. hydrophilic/hydrophobic either at the molecular or macromolecular states.[20]

Conclusion

The relationship, which comes from analysis of thick films (about 1- 2 mm thick), between the microstructure of microgels and the mechanical strength of microgel-based films was successfully put into evidence thanks to dynamic mechanical measurements at low strain, uniaxial tests at high deformation and AFM observations. Indeed, the looser and less crosslinked structure of MBA microgels not only leads to softer films but also enhances the inter-diffusion of chain at the particle interface, leading to higher strains at rupture. The structural characterization of the water-soluble polymer by SEC has demonstrated higher molecular masses for the polymer resulting from the MBA crosslinking than the OEGDA one.

This finding strengthens the idea that the looser structure of MBA microgels was due to a higher portion of the crosslinker reacting with the water-soluble chains instead of the microgels particles themselves. Finally, blended films were successfully formed by mixing microgels and water-soluble polymers in a controlled ratio with water-soluble polymer content till 100%. AFM images demonstrate that the structure of blended films resembles to the one of a composite material with hard fillers (microgels) incorporated in a soft matrix (water-soluble polymers). The addition of water-soluble polymer allows to vary the elastic modulus of classic microgel films (G' ranging from $\approx 1x10^3$ to $\approx 1x10^5$ MPa) without changing the elongational properties of the films. This valuable finding is attributed to the branched and/or crosslinked structure of water-soluble polymers and their high compatibility with microgels. As corona of dangling chains has a major impact on the properties of the film, as a perspective, one can consider neutron techniques or super resolution microscopy study to well reveal internal structure of the microgels.

Regarding the usefulness of self-assembled microgel films, *i.e.* raw or purified ones, they clearly exhibit the ability for different medical applications as delivery patches systems or protective films.

Associated contents

- AFM mappings of OEGDA-based microgels films

- Strains and extensional viscosities at rupture for different strain rates of MBA- and OEGDA-based microgel films

- Strain at break, stress at break and fracture energy of MBA- and OEGDA-crosslinked microgel films

- Molar mass and gyration radius as a function of elution volume of MBA and OEGDA-based water-soluble polymers

- frequency sweep curves and average extensional viscosity curves for OEGDA blended films

- Hencky strain at break and extensional viscosity at break *versus* microgel for OEGDA and MBA blended films.

Author information

Corresponding Author

*E-mail: christophe.derail@univ-pau.fr; Tel: +33 559407706 and laurent.billon@univ-pau.fr

Author Contributions

The manuscript was written through contributions of all authors. All authors have given approval to the final version of the manuscript.

Conflicts of interest

The authors declared no conflict of interest.

Acknowledgements

E. Dieuzy is grateful to URGO RID, LVMH and the Région Nouvelle Aquitaine, convention 2016-1R10204-00007186 – THESE for her PhD financial support. This work benefits from the financial support of the French National Research Agency, conventions Labcom ANR-14-LAB3-0003-01 and ANR-17-LCCO-0003-01. The authors thank Pr. Brunol Grassl and Dr. Nathalie Andreu for the discussion related to the SEC measurements.

References

(1) Steward, P. A.; Hearn, J.; Wilkinson, M. C. An Overview of Polymer Latex Film Formation and Properties. *Advances in Colloid and Interface Science* **2000**, *86* (3), 195–267.

(2) Santos, F. D. D.; Leibler, L. Large Deformation of Films from Soft-Core/Hard-Shell Hydrophobic Latices. *Journal of Polymer Science Part B: Polymer Physics* **2003**, *41* (3), 224–234.

(3) Deplace, F.; Rabjohns, M. A.; Yamaguchi, T.; Foster, A. B.; Carelli, C.; Lei, C.-H.; Ouzineb, K.; Keddie, J. L.; Lovell, P. A.; Creton, C. Deformation and Adhesion of a Periodic Soft–Soft Nanocomposite Designed with Structured Polymer Colloid Particles. *Soft Matter* **2009**, *5* (7), 1440–1447.

(4) Lepizzera, S.; Lhommeau, C.; Dilger, G.; Pith, T.; Lambla, M. Film-Forming Ability and Mechanical Properties of Coalesced Latex Blends. *Journal of Polymer Science Part B: Polymer Physics* **1997**, *35* (13), 2093–2101.

(5) Baït, N.; Grassl, B.; Derail, C.; Benaboura, A. Hydrogel Nanocomposites as Pressure-Sensitive Adhesives for Skin-Contact Applications. *Soft Matter* **2011**, *7* (5), 2025–2032.

(6) Oberdisse, J. Structure and Rheological Properties of Latex−Silica Nanocomposite Films: Stress−Strain Isotherms. *Macromolecules* **2002**, *35* (25), 9441–9450.

(7) Pelton, R. Temperature-Sensitive Aqueous Microgels. *Adv Colloid Interface Sci* **2000**, *85* (1), 1–33.

(8) Pelton, R. H.; Chibante, P. Preparation of Aqueous Latices with N-Isopropylacrylamide. *Colloids and Surfaces* **1986**, *20* (3), 247–256.

(9) Plamper, F. A.; Richtering, W. Functional Microgels and Microgel Systems. *Acc. Chem. Res.* **2017**, *50* (2), 131–140.

(10) Karg, M.; Pich, A.; Hellweg, T.; Hoare, T.; Lyon, L. A.; Crassous, J. J.; Suzuki, D.; Gumerov, R. A.; Schneider, S.; Potemkin, Igor. I.; Richtering, W. Nanogels and Microgels: From Model Colloids to Applications, Recent Developments, and Future Trends. *Langmuir* **2019**, *35* (19), 6231–6255.

(11) Serpe, M. J.; Jones, C. D.; Lyon, L. A. Layer-by-Layer Deposition of Thermoresponsive Microgel Thin Films. *Langmuir* **2003**, *19* (21), 8759–8764.

(12) Serpe, M. J.; Yarmey, K. A.; Nolan, C. M.; Lyon, L. A. Doxorubicin Uptake and Release from Microgel Thin Films. *Biomacromolecules* **2005**, *6* (1), 408–413.

(13) Wong, J. E.; Díez-Pascual, A. M.; Richtering, W. Layer-by-Layer Assembly of Polyelectrolyte Multilayers on Thermoresponsive P(NiPAM-Co-MAA) Microgel: Effect of Ionic Strength and Molecular Weight. *Macromolecules* **2009**, *42* (4), 1229–1238.

(14) Li, X.; Serpe, M. J. Understanding and Controlling the Self-Folding Behavior of Poly (N-Isopropylacrylamide) Microgel-Based Devices. *Advanced Functional Materials* **2014**, *24* (26), 4119–4126.

(15) Hu, L.; Sarker Avijeet, K.; Islam Molla, R.; Li, X.; Lu, Z.; Serpe Michael, J. Poly (N-isopropylacrylamide) Microgel-based Assemblies. *Journal of Polymer Science Part A: Polymer Chemistry* **2013**, *51* (14), 3004–3020.

(16) Burmistrova, A.; von Klitzing, R. Control of Number Density and Swelling/Shrinking Behavior of P(NIPAM–AAc) Particles at Solid Surfaces. *J. Mater. Chem.* **2010**, *20* (17), 3502.

(17) Nash, M. E.; Carroll, W. M.; Foley, P. J.; Maguire, G.; Connell, C. O.; Gorelov, A. V.; Beloshapkin, S.; Rochev, Y. A. Ultra-Thin Spin Coated Crosslinkable Hydrogels for Use in Cell Sheet Recovery—Synthesis, Characterisation to Application. *Soft Matter* **2012**, *8* (14), 3889.

(18) Sanzari, I.; Buratti, E.; Huang, R.; Tusan, C. G.; Dinelli, F.; Evans, N. D.; Prodromakis, T.; Bertoldo, M. Poly(N-Isopropylacrylamide) Based Thin Microgel Films for Use in Cell Culture Applications. *Sci Rep* **2020**, *10* (1), 6126.

(19) Zhou, J.; Wang, G.; Marquez, M.; Hu, Z. The Formation of Crystalline Hydrogel Films by Self-Crosslinking Microgels. *Soft Matter* **2009**, *5* (4), 820–826.

(20) Sonzogni, A. S.; Passeggi, M. C. G.; Wedepohl, S.; Calderón, M.; Gugliotta, L. M.; Gonzalez, V. D. G.; Minari, R. J. Thermoresponsive Nanogels with Film-Forming Ability. *Polym. Chem.* **2018**, *9* (8), 1004–1011.

(21) Boularas, M.; Radji, S.; Gombart, E.; Tranchant, J.-F.; Alard, V.; Billon, L. Functional Film by Trigger-Free Self-Assembly of Adhesive Soft Microgels at Skin Temperature. *Materials & Design* **2018**, *147*, 19–27.

(22) Boularas, M.; Deniau-Lejeune, E.; Alard, V.; Tranchant, J.-F.; Billon, L.; Save, M.

Dual Stimuli-Responsive Oligo(Ethylene Glycol)-Based Microgels: Insight into the Role of Internal Structure in Volume Phase Transitions and Loading of Magnetic Nanoparticles to Design Stable Thermoresponsive Hybrid Microgels. *Polymer Chemistry* **2016**, *7* (2), 350–363.

(23) Dieuzy, E. Relationship between Structural and Rheological Properties of Dual-Stimuli Responsive Microgel Films for Cosmetic and Biomedical Applications. Thèse de doctorat en Polymères, Université de Pau et des Pays de l'adour, 2019.

(24) Dieuzy, E.; Aguirre, G.; Auguste, S.; Chougrani, K.; Alard, V.; Billon, L.; Derail, C. Microstructure-Driven Self-Assembly and Rheological Properties of Multi-Responsive Soft Microgel Suspensions. *Journal of Colloid and Interface Science* **2021**, *581*, 806–815.

(25) Aguirre, G.; Khoukh, A.; Taboada, P.; Chougrani, K.; Alard, V.; Billon, L. Smart Self-Assembled Microgel Films as Encapsulating Carriers for UV-Absorbing Molecules. *Polymer Chemistry* **2018**, *9* (10), 1155–1159.

(26) Boularas, M.; Gombart, E.; Tranchant, J.; Billon, L.; Save, M. Design of Smart Oligo(Ethylene Glycol)-Based Biocompatible Hybrid Microgels Loaded with Magnetic Nanoparticles. *Macromolecular Rapid Communications* **2015**, *36* (1), 79–83.

(27) Aguirre, G.; Khoukh, A.; Chougrani, K.; Alard, V.; Billon, L. Dual-Responsive Biocompatible Microgels as High Loaded Cargo: Understanding of Encapsulation/Release Driving Forces by NMR NOESY. *Polymer Chemistry* **2018**, *9* (6), 757–768.

(28) Ferry, J. D. *Viscoelastic Properties of Polymers*, 3d ed.; Wiley: New York, 1980.

(29) Mejia, A.; Rodriguez, L.; Schmitt, C.; Andreu, N.; Favéro, C.; Braun, O.; Dupuis, G.; Deniau, E.; Reynaud, S.; Grassl, B. Synthesis and Viscosimetric Behavior of Poly(Acrylamide-Co-2-Acrylamido-2-Methylpropanesulfonate) Obtained by Conventional and Adiabatic Gel Process via RAFT/MADIX Polymerization. *ACS Omega* **2019**, *4* (6), 11119–11125.

(30) Zosel, A.; Ley, G. Influence of Crosslinking on Structure, Mechanical Properties, and Strength of Latex Films. *Macromolecules* **1993**, *26* (9), 2222–2227.

(31) Pinenq, P.; Winnik, M. A.; Ernst, B.; Juhué, D. Polymer Diffusion and Mechanical Properties of Films Prepared from Crosslinked Latex Particles. *Journal of Coatings Technology* **2000**, *72* (903), 45–61.

(32) Degrandi-Contraires, E.; Udagama, R.; Bourgeat-Lami, E.; McKenna, T.; Ouzineb, K.; Creton, C. Mechanical Properties of Adhesive Films Obtained from PU−Acrylic Hybrid Particles. *Macromolecules* **2011**, *44* (8), 2643–2652.

(33) Udagama, R.; Degrandi-Contraires, E.; Creton, C.; Graillat, C.; McKenna, T. F. L.; Bourgeat-Lami, E. Synthesis of Acrylic−Polyurethane Hybrid Latexes by Miniemulsion Polymerization and Their Pressure-Sensitive Adhesive Applications. *Macromolecules* **2011**, *44* (8), 2632–2642.

(34) Ward, I. M.; Sweeney, J. *An Introduction to the Mechanical Properties of Solid Polymers*, 2nd ed.; Wiley: Chichester, West Sussex, England, 2004.

(35) Sentmanat, M.; Wang, B. N.; McKinley, G. H. Measuring the Transient Extensional Rheology of Polyethylene Melts Using the SER Universal Testing Platform. *Journal of*

Rheology **2005**, *49* (3), 585–606.

(36) Paillet, S.; Roncin, A.; Clisson, G.; Pembouong, G.; Billon, L.; Derail, C.; Save, M. Combination of Nitroxide-mediated Polymerization and SET-LRP for the Synthesis of High Molar Mass Branched and Star-branched Poly(N-butyl Acrylate) Characterized by Size Exclusion Chromatography and Rheology. *Journal of Polymer Science Part A: Polymer Chemistry* **2012**, *50* (14), 2967–2979.

(37) Stange, J.; Münstedt, H. Effect of Long-Chain Branching on the Foaming of Polypropylene with Azodicarbonamide. *Journal of Cellular Plastics* **2006**, *42* (6), 445–467.

(38) Ajji, A.; Sammut, P.; Huneault, M. A. Elongational Rheology of LLDPE / LDPE Blends. *Journal of Applied Polymer Science* **2003**, *88* (14), 3070–3077.

(39) Tabatabaei Seyed, H.; Carreau Pierre, J.; Ajji, A. Rheological Properties of Blends of Linear and Long-chain Branched Polypropylenes. *Polymer Engineering & Science* **2009**, *50* (1), 191–199.

(40) Yamaguchi, M.; Suzuki, K.-I.; Maeda, S. Enhanced Strain Hardening in Elongational Viscosity for HDPE/Crosslinked HDPE Blend. I. Characteristics of Crosslinked HDPE. *Journal of Applied Polymer Science* **2002**, *86* (1), 73–78.

(41) Wu, C.; Zhou, S. Laser Light Scattering Study of the Phase Transition of Poly(N-Isopropylacrylamide) in Water. 1. Single Chain. *Macromolecules* **1995**, *28* (24), 8381–8387.

(42) Mourran, A.; Wu, Y.; Gumerov, R. A.; Rudov, A. A.; Potemkin, I. I.; Pich, A.; Möller, M. When Colloidal Particles Become Polymer Coils. *Langmuir* **2016**, *32* (3), 723–730.

(43) Siviour, C. R.; Jordan, J. L. High Strain Rate Mechanics of Polymers: A Review. *J. dynamic behavior mater.* **2016**, *2* (1), 15–32.

(44) Cai, T.; Wang, G.; Thompson, S.; Marquez, M.; Hu, Z. Photonic Hydrogels with Poly(Ethylene Glycol) Derivative Colloidal Spheres as Building Blocks. *Macromolecules* **2008**, *41* (24), 9508–9512.

(45) Yu, B.; Kang, S.-Y.; Akthakul, A.; Ramadurai, N.; Pilkenton, M.; Patel, A.; Nashat, A.; Anderson, D. G.; Sakamoto, F. H.; Gilchrest, B. A.; Anderson, R. R.; Langer, R. An Elastic Second Skin. *Nature Materials* **2016**, *15* (8), 911–918.

(46) Renvoise, J.; Burlot, D.; Marin, G.; Derail, C. Peeling of PSAs on Viscoelastic Substrates: A Failure Criterion. *The Journal of Adhesion* **2007**, *83* (4), 403–416.

(47) Renvoise, J.; Burlot, D.; Marin, G.; Derail, C. Adherence Performances of Pressure Sensitive Adhesives on a Model Viscoelastic Synthetic Film: A Tool for the Understanding of Adhesion on the Human Skin. *Int J Pharm* **2009**, *368* (1–2), 83–88.

(48) Kalra, A.; Lowe, A.; Al-Jumaily, A. Mechanical Behaviour of Skin: A Review. *J Material Sci Eng* **2016**, *5* (4).

(49) Ní Annaidh, A.; Bruyère, K.; Destrade, M.; Gilchrist, M. D.; Otténio, M. Characterization of the Anisotropic Mechanical Properties of Excised Human Skin. *Journal of the Mechanical Behavior of Biomedical Materials* **2012**, *5* (1), 139–148.

(50) Gallagher, A.; Ní Annaidh, A.; Bruyère-Garnier, K.; et al. Dynamic Tensile Properties

of Human Skin; International Research Council on the Biomechanics of Injury, 2012; pp 12–14.

(51) Lepizzera, S.; Scheer, M.; Fond, C.; Pith, T.; Lambla, M.; Lang, J. Coalesced Core/Shell Latex Films under Elongation Imaged by Atomic Force Microscopy. *Macromolecules* **1997**, *30* (25), 7953–7957.

(52) Lepizzera, S.; Pith, T.; Fond, C.; Lambla, M. Mechanical Behavior at Finite Strain of Coalesced Core/Shell Latex Films. *Macromolecules* **1997**, *30*, 7945–7952.

(53) Bitar, A.; Fessi, H.; Elaissari, A. Synthesis and Characterization of Thermally and Glucose-Sensitive Poly N-Vinylcaprolactam-Based Microgels. *J Biomed Nanotechnol* **2012**, *8* (5), 709–719.

(54) Kratochvíl, P.; Netopilík, M. The Effect of Nanoparticle Nonuniformity on the Ratio of Gyration and Hydrodynamic Radiuses. *International Journal of Polymer Analysis and Characterization* **2017**, *22* (2), 112–117.

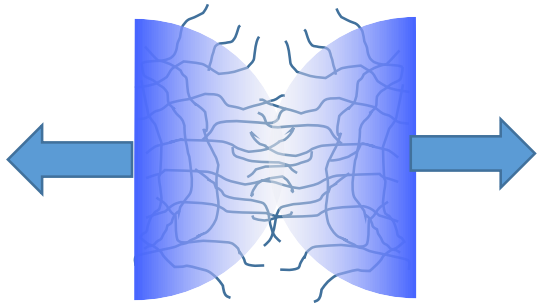

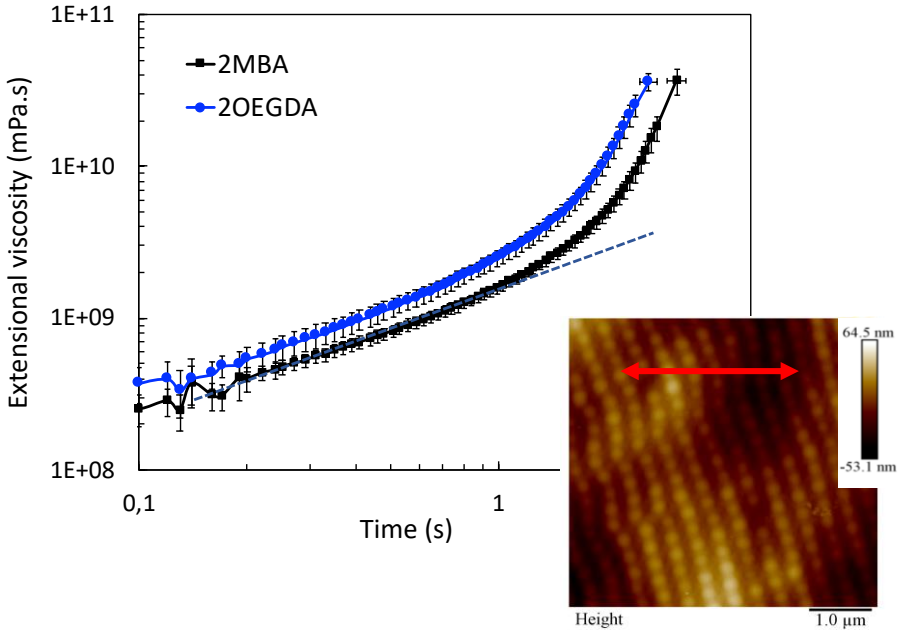
1E+11
1E+10
1E+09
1E+08
Extensional viscosity (mPa.s)
2MBA
2OEGDA
0,1
1
Time (s)
64.5 nm
-53.1 nm
Height
1.0 µm